minerals

MDPI

Article

Preferential Elimination of Ba^{2+} through Irreversible Biogenic Manganese Oxide Sequestration

Yukinori Tani [1,2,*], Satomi Kakinuma [1], Jianing Chang [2], Kazuya Tanaka [3] and Naoyuki Miyata [4]

1 Department of Environmental and Life Sciences, School of Food and Nutritional Sciences, University of Shizuoka, 52-1 Yada, Shizuoka 422-8526, Japan; st.kakinuma@gmail.com
2 Department of Environmental Health Sciences, Graduate School of Nutritional and Environmental Sciences, University of Shizuoka, 52-1 Yada, Shizuoka 422-8526, Japan; jianing_ch0802@sina.com
3 Advanced Science Research Center, Japan Atomic Energy Agency, Tokai, Ibaraki 319-1195, Japan; tanaka.kazuya@jaea.go.jp
4 Department of Biological Environment, Akita Prefectural University, Shimoshinjo-Nakano, Akita 010-0195, Japan; nmiyata@akita-pu.ac.jp
* Correspondence: taniy@u-shizuoka-ken.ac.jp; Tel.: +81-54-264-5797

Abstract: Biogenic manganese oxides (BMOs) formed in a culture of the Mn(II)-oxidizing fungus *Acremonium strictum* strain KR21-2 are known to retain enzymatic Mn(II) oxidation activity. Consequently, these are increasingly attracting attention as a substrate for eliminating toxic elements from contaminated wastewaters. In this study, we examined the Ba^{2+} sequestration potential of enzymatically active BMOs with and without exogenous Mn^{2+}. The BMOs readily oxidized exogenous Mn^{2+} to produce another BMO phase, and subsequently sequestered Ba^{2+} at a pH of 7.0, with irreversible Ba^{2+} sequestration as the dominant pathway. Extended X-ray absorption fine structure spectroscopy and X-ray diffraction analyses demonstrated alteration from turbostratic to tightly stacked birnessite through possible Ba^{2+} incorporation into the interlayer. The irreversible sequestration of Sr^{2+}, Ca^{2+}, and Mg^{2+} was insignificant, and the turbostratic birnessite structure was preserved. Results from competitive sequestration experiments revealed that the BMOs favored Ba^{2+} over Sr^{2+}, Ca^{2+}, and Mg^{2+}. These results explain the preferential accumulation of Ba^{2+} in natural Mn oxide phases produced by microbes under circumneutral environmental conditions. These findings highlight the potential for applying enzymatically active BMOs for eliminating Ba^{2+} from contaminated wastewaters.

Keywords: biogenic manganese oxide; Mn(II) oxidizing fungi; sequestration of barium(II) ion; *Acrenonium strictum*; birnessite

Citation: Tani, Y.; Kakinuma, S.; Chang, J.; Tanaka, K.; Miyata, N. Preferential Elimination of Ba^{2+} through Irreversible Biogenic Manganese Oxide Sequestration. *Minerals* **2021**, *11*, 53. https://doi.org/10.3390/min11010053

Received: 23 December 2020
Accepted: 6 January 2021
Published: 7 January 2021

1. Introduction

Barium is a toxic alkaline earth metal [1,2], and Ba^{2+} levels have been elevated in many aquatic environments by anthropogenic activities such as mining [3], coal seam gas utilization [4], and shale gas extraction [5,6]. These enhanced Ba levels threaten humans and ecosystems worldwide. Therefore, developing a cost-effective Ba^{2+} remediation systems requires urgent attention.

In aquatic and terrestrial environments, manganese (Mn) oxide phases readily accumulate Ba^{2+} and other heavy metal ions such as Ni^{2+}, Co^{2+}, and Zn^{2+}. The preferential accommodation of Ba^{2+} in the tunnels of tectomanganates such as hollandite (2 × 2) and romanechite (2 × 3) partly explains Ba^{2+} accumulation in natural Mn oxide phases [7–9]. Phyllomanganates such as birnessite and buserite (vernadite) also accumulate Ba^{2+} under certain environmental conditions [10–15], although the underlying mechanisms for Ba^{2+} accumulation in manganese oxide phases remain uncertain.

Under circumneutral pH conditions, bacterial and fungal Mn oxide formation enzymatically proceeds faster than heterogeneous Mn(II) oxidation catalyzed by mineral

surfaces [16–18]. The formation of biogenic Mn oxides (BMOs) serves in scavenging heavy metal cations including Zn^{2+}, Ni^{2+}, Co^{2+}, and Pb^{2+} from aquatic environments because of the high sequestration affinity and capacity of BMOs [19–28].

According to previous studies [29–31], fungal BMOs produced by *Acremonium strictum* KR21-2 maintain the activity of an Mn(II)-oxidizing enzyme in the oxide phase, and effectively oxidize exogenous Mn^{2+} to form another BMO phase. This process significantly enhances the efficiency of heavy metal [32–35] and rare-earth metal [36,37] sequestration by providing new sorption sites and minimizing competition for exogenous Mn^{2+} sorption. In addition, enzymatically active BMOs improve the indirect oxidation efficiencies of As(III) to As(V) [30], Co(II) to Co(III) [33], and Cr(III) to Cr(VI) [38] through continuous reoxidation of reduced Mn^{2+}, which is one of the causes of surface passivation. Consequently, in addition to the high sequestration capacity and oxidizing ability, enzymatically active BMOs exhibit a potential for a continuous remediation of contaminated wastewaters as well as metal recovery.

The aims of this study were to examine the Ba^{2+} sequestration process associated with enzymatic BMO formation and to elucidate factors for the preferential accumulation of this ion in Mn oxide phases in the environment. The BMO alteration linked to the Ba^{2+} sequestration is also discussed relative to the sequestration reversibility and selectivity for alkali earth metal ions such as Sr^{2+}, Ca^{2+}, and Mg^{2+}. The results of this study demonstrate the potential application of enzymatically active BMOs for Ba^{2+} removal from contaminated wastewaters.

2. Materials and Methods

A. strictum KR21-2, which enzymatically oxidizes Mn(II) to BMOs [39–41], was incubated at 25 °C in a HAY liquid medium (pH of 7.0) supplemented with 1 mM Mn^{2+}, as described previously [29,32–34], slightly modified by using $Mn(NO_3)_2$ instead of $MnSO_4$. After 72 h of incubation, BMOs with fungal mycelia were harvested and washed thrice with 20 mM 4-(2-hydroxyethyl)–1–piperazineethanesulphonic acid (HEPES) buffer (pH of 7.0 adjusted using NaOH). These served as the "newly formed BMOs" for Ba^{2+} sequestration experiments within 1 h of washing (denoted as "newly formed BMO").

In the sequestration experiments, all metal ions involved (Mn^{2+}, Ba^{2+}, Sr^{2+}, Ca^{2+}, and Mg^{2+}) were as nitrate salts because Ba^{2+} readily precipitates with SO_4^{2-} (the solubility product, K_{sp}, of $BaSO_4$ is $10^{-9.97}$ [42]). The enzymatically active newly formed BMOs (1 mM as Mn) were mixed with 0–10 mM $Ba(NO_3)_2$ with or without 1 mM $Mn(NO_3)_2$ in 20 mM HEPES buffer (50 mL) at a pH of 7.0 (adjusted using NaOH) under air-equilibrated (aerobic) conditions at 25 °C on a reciprocal shaker at 105 strokes·min^{-1} (NR–10, Taitec, Nagoya, Aichi, Japan). To maintain aerobic conditions, we used 100 mL Erlenmeyer flasks with cotton stoppers. This procedure was performed thrice, with the bathing solution renewed every 24 h. To elucidate the effects of the Mn(II) oxidase activity in the BMOs, we inactivated the associated Mn(II) oxidase by heating the newly formed BMOs for 2 h in a water bath (Thermo Minder Mini-80, Taitec, Nagoya, Aichi, Japan) at 85 °C [29], followed by cooling of the samples to room temperature at around 20 °C (denoted as "heated BMO" hereafter). These cooled samples were collected, washed thrice with a 20 mM HEPES buffer at pH of 7.0, and used in the Ba^{2+} sequestration experiments under aerobic conditions. To compare the sequestration properties of the alkaline earth metal ions, we also conducted experiments with solutions of Sr^{2+}, Ca^{2+}, and Mg^{2+} in the 20 mM HEPES buffer. For competitive sequestration experiments, newly formed BMOs were treated thrice in mixed solutions of Ba^{2+} with Sr^{2+}, Ca^{2+}, or Mg^{2+}, and with or without exogenous Mn^{2+}. In all sequestration experiments, supernatants were sampled at 0, 2, 8, 16, and 24 h for each treatment and separated using a centrifugal filter unit (Durapore PVDF 0.1 μm, Merk Millipore, Burlington, MA, USA; 12,000× *g* for 2 min). The dissolved metal concentrations of the supernatants were measured using a 730-ES inductivity coupled plasma atomic emission spectrometer (ICP-AES, Agilent Technology, Santa Clara, CA, USA).

The two-step extraction protocol in this study involved using aqueous 10 mM $Cu(NO_3)_2$ (pH of 4.8) and 50 mM hydroxylamine hydrochloride for speciation of the Ba^{2+} and Mn^{2+} sequestered by the BMOs, as described previously [29,32–34]. This extraction sequence commonly serves for fractionating adsorbed Mn(II) and oxidized Mn from BMOs [43–45]. The Ba^{2+} and other alkaline earth metal ion fractions dissolved in aqueous $Cu(NO_3)_2$, and the subsequent hydroxylamine hydrochloride extracts were termed as exchangeable (reversible) and reducible (irreversible) fractions, respectively. The metal concentrations in the extracts were also determined using ICP-AES after dilution with 1.0 M HNO_3. The total metal ions extracted via this two-step extraction sequence is hereafter referred to as "solid". All the sequestration and extraction experiments were conducted in triplicate (n = 3), and data in the figures and tables are shown as mean ± standard deviation.

X-ray diffraction (XRD) measurements were performed for the BMOs using a Rigaku Rint2500 diffractometer (Akishima, Tokyo, Japan) involving CuKα radiation at 26 mA and 40 kV. Lyophilized BMO samples were placed on a glass holder and scanned over a 2θ range of 5–70° at 1.0° min^{-1} using a 0.02° step interval. The diffractograms were smoothed using a 10-point moving average to enhance the display of broad peaks.

Manganese K-edge extended X-ray absorption fine structure (EXAFS) data for the BMO samples were obtained at the BL12C in the Photon Factory, KEK (Tsukuba, Japan). Lyophilized BMO samples were diluted and adequately mixed with boron nitride (BN). After homogenization, the mixed BMO–BN powders were pressed into discs of appropriate thicknesses for EXAFS measurements in the transmission mode. The intensities of the incident and transmitted X-rays were monitored at room temperature using ionization chambers. Conversely, Barium K-edge EXAFS data for the BMOs treated with Ba^{2+} were measured at the BL01B1 in the SPring-8 facility (Hyogo, Japan). The lyophilized samples for the Ba-edge EXAFS were also pressed to form discs, without BN dilution. The EXAFS data were also generated in the transmission mode using ionization chambers and analyzed using ver. 2.5.9 of REX2000 (Rigaku Co. Ltd., Akishima, Tokyo, Japan).

3. Results and Discussion

3.1. Exogenous Mn^{2+} Oxidation by Newly Formed BMOs

Under aerated (air-equilibrated) conditions, the newly formed BMOs (1 mM Mn) readily converted 1 mM exogenous Mn^{2+} to solid phase Mn in 20 mM HEPES at a pH of 7.0 (cumulative sequestration efficiency > 98.7 ± 0.1%) and subsequently produced another solid phase (Figure S1A and Table S1). Two-step extraction experiments confirmed that these solid phases mainly comprised reducible (oxidized) Mn (>84.2 ± 0.1%) with minor (<15.8 ± 0.1%) exchangeable Mn^{2+} after every 24 h in the repeated treatment (Figure S1B). The XRD patterns of the newly formed BMOs are characterized by broad peaks for the (001) and (002) basal reflections at ~7.4 and ~3.6 Å, respectively (Figure S2a), indicating a turbostratic birnessite structure [45]. These patterns were maintained even after repeated exogenous Mn^{2+} oxidation (Figure S2b–d).

3.2. Ba^{2+} Sequestration by Newly Formed or Heated BMOs with Exogenous Mn^{2+}

After adding newly formed BMOs (1 mM as Mn) to a mixture of 1 mM $Mn(NO_3)_2$ and 1 mM $Ba(NO_3)_2$ (20 mM HEPES at a pH of 7.0), the exogenous Mn^{2+} concentrations decreased over time, with >99% subsequently converted to solid Mn upon termination of each treatment (Figure 1A and Table S1). Two-step extraction data also revealed that oxidized (reducible) Mn dominated the solid Mn phase throughout the repeated treatment (93.4 ± 0.1% to 94.7 ± 0.5%) (Figure 1D), indicating active Mn oxide formation by the newly formed BMOs. In fact, dissolved Ba^{2+} was efficiently sequestered, with the content reducing from 27.0 ± 0.5% upon the initial treatment to 10.0 ± 0.3% after the third treatment (Figure 1A). The cumulative Ba^{2+} concentration increased by up to 0.45 ± 0.00 mM (Figure 1C) (the cumulative efficiency was 16.1 ± 0.0%, Table S1). The molar ratio of the sequestered Ba^{2+} relative to the oxidized Mn (Ba^{2+}_{seq}/Mn_{oxide}) was 11.9 ± 0.1 mol % at the end of the repeated treatment.

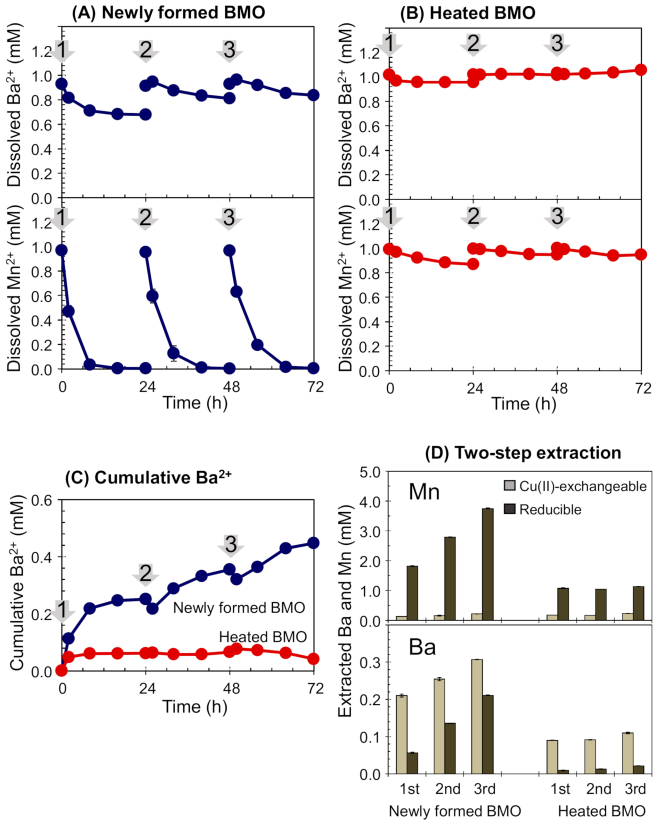

Figure 1. Illustration of the repeated treatment of the (**A**) newly formed and (**B**) heated biogenic manganese oxides (1 mM Mn) with mixtures of 1 mM $Ba(NO_3)_2$ and 1 mM $Mn(NO_3)_2$ in 20 mM 4-(2-hydroxyethyl)–1–piperazineethanesulphonic acid (HEPES) (pH of 7.0). (**C**) Cumulative concentration of the sequestered Ba^{2+} and (**D**) exchangeable and reducible Ba and Mn in the solid phases, assessed via the two-step extraction. Bathing solutions were renewed every 24 h (indicated by arrows).

In contrast, upon treatment with heated BMOs, the exogenous Mn^{2+} slightly reduced (Figure 1B), thereby minimally increasing the solid Mn phase (Figure 1D). This behavior is attributed to the lack of enzymatic Mn(II) oxidation ability of the heated BMOs [29]. The dissolved Ba^{2+} concentration also slightly decreased, producing a minor cumulative Ba^{2+} sequestration of 0.04 ± 0.01 mM (efficiency ≈ 1.4%; Figure 1C). Here, a significantly lower $Ba^{2+}{}_{seq}/Mn_{oxide}$ ratio (3.7 ± 0.5 mol %) was obtained, indicating competitive sorption of unreacted exogenous Mn^{2+} (Figure 1B) and Ba^{2+} on the BMO surface, as previously demonstrated for heavy metal ion sequestration [32,34]. Consequently, the enzymatic Mn^{2+} oxidation ability enhanced the Ba^{2+} sequestration efficiency not only by preparing new accommodation sites, for example, a new BMO phase, but also by minimizing the impact of exogenous Mn^{2+} as a sorption competitor. In fact, newly formed BMOs without exogenous Mn^{2+} produced the highest $Ba^{2+}{}_{seq}/Mn_{oxide}$ ratio of 19.5 ± 0.9 mol %, with the cumulative sequestered Ba^{2+} concentration limited to 0.19 ± 0.01 mM (Figure S3 and Table S1), which is significantly lower than that with 1 mM exogenous Mn^{2+} (0.45 ± 0.00 mM; Figure 1C).

Interestingly, the two-step extraction data revealed Ba^{2+} sequestration reversibility differences between the newly formed and heated BMOs. In the newly formed BMOs, the total sequestered Ba^{2+} contained up to 40.7 ± 0.1% irreversible Ba^{2+} (extracted as the reducible phase) (Figure 1D and Table S1), whereas for the heated BMOs, the sequestered Ba^{2+} was mainly extracted as exchangeable Ba^{2+} (90.3 ± 0.9 to 83.6 ± 0.0%) during the repeated treatment (Figure 1D). Similar trends were observed for initial Ba^{2+} concentrations ranging from 0.15 to 10 mM and 1 mM exogenous Mn^{2+} (Figure 2). In fact, at initial Ba^{2+} concentrations of 0.15, 3, and 10 mM, irreversible Ba^{2+} represents 58.3 ± 1.2%, 44.1 ± 0.6%, and 44.4 ± 0.6% sequestration on the newly formed BMOs, respectively (Figure 2 and

Table S1). However, for the Ba^{2+} sequestered by the heated BMOs, exchangeable Ba^{2+} makes up 76.3 ± 0.5%, 82.1 ± 0.5%, and 82.5 ± 0.4% for corresponding initial Ba^{2+} concentrations (Figure 2 and Table S1). In addition, even for the newly formed BMOs, irreversible Ba^{2+} incorporation is scarce without exogenous Mn^{2+} addition, with >93% of the sequestered Ba^{2+} as exchangeable Ba^{2+} (Figure S3D).

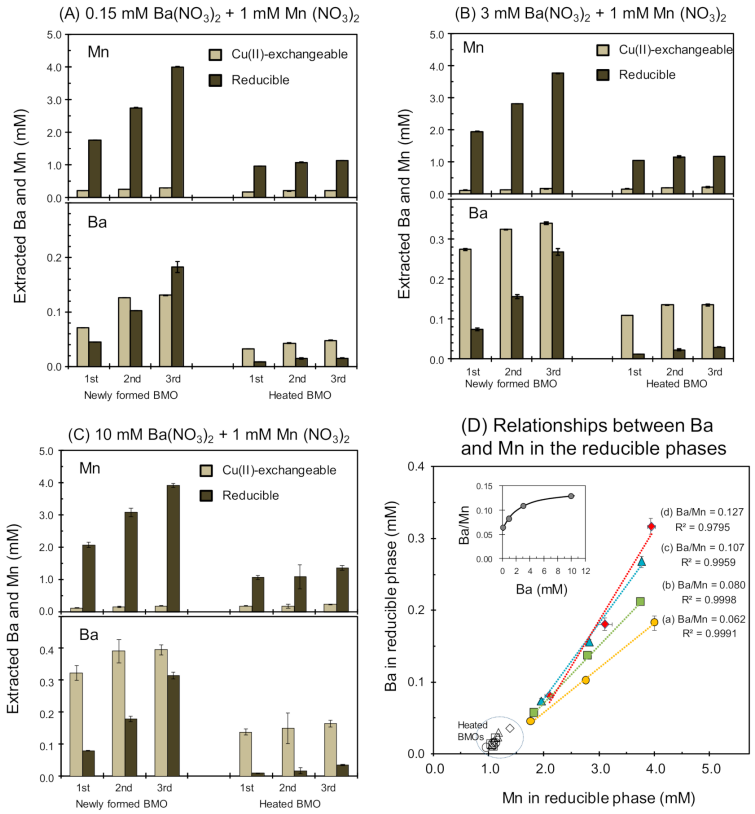

Figure 2. Diagram showing the two-step extraction of Ba^{2+} and Mn from the newly formed and heated biogenic manganese oxides through repeated treatment with mixtures of (**A**) 0.15 mM, (**B**) 3 mM, and (**C**) 10 mM $Ba(NO_3)_2$ with 1 mM $Mn(NO_3)_2$ in 20 mM HEPES (pH of 7.0). (**D**) Plot displaying linear relationships between the extracted Ba and Mn in reducible phases, with the inset showing the Ba/Mn molar ratios as a function of the initial Ba^{2+} concentration.

Linear correlations between the amounts of irreversible Ba^{2+} and reducible (oxidized) Mn in the solid phase (R^2 > 0.97) were observed throughout the repeated treatments (Figure 2D). From the slopes of the linear relationship curves, molar ratios of the irreversible Ba^{2+} to the additional oxidized Mn phase from the exogenous Mn^{2+} increased from 0.062, 0.080, and 0.107 to 0.127 as the initial Ba^{2+} concentrations increased from 0.15, 1, and 3 to 10 mM, respectively (Figure 2D inset). Considering the incorporation of irreversible Ba^{2+} into the additional Mn oxide phase, 16.2, 12.5, 9.4, and 7.9 moles of oxidized Mn accommodated 1 mole of irreversible Ba^{2+}, on average, as the initial Ba^{2+} concentrations changed from 0.15, 1, and 3 to 10 mM, respectively. Although isomorphic substitution with structural Mn^{4+} is reported to cause irreversible sequestration of Ni^{2+} [34], this is impossible for Ba^{2+} because of its significantly higher ionic radius (1.49–1.75 Å [46]) compared to that of Mn^{4+} (0.53–0.67 Å [46]).

3.3. BMO Alteration from Turbostratic to Tightly Stacked Birnessite

The Mn K-edge EXAFS data for the newly formed BMOs (untreated) were similar to those of chemically synthesized δ-MnO_2 (Figure 3). This is consistent with the fact that the original BMOs were turbostratic analogues of birnessite [47]. Even after adding the exogenous Mn^{2+}, the newly formed BMOs maintained the EXAFS oscillations throughout

the repeated treatment in 10 mM Ba^{2+} (Figure 3). This indicated no remarkable alteration in the structural alignment of Mn in the resultant BMOs, although the Ba^{2+} sequestration reversibility largely became irreversible. This behavior is inconsistent with the formation of tectomanganates such as hollandite (2 × 2) and romanechite (2 × 3). These naturally occurring Mn oxides are considered the most suitable for accommodating Ba^{2+} because of their tunnel structures [7,9,11,28]. Therefore, we inferred that under the experimental conditions in this study, the coexisting Ba^{2+} failed to directly stimulate tectomanganate formation through enzymatic Mn(II) oxidation. However, some studies have reported direct tectomanganate formation from biogenic Mn oxide processes. Webb et al. [48], for example, reported pseudo-tunnel structures (todorokite-like), with $U^{VI}O_2^{2+}$ serving as a template ion, during Mn oxide biogenesis by *Bacillus* sp. SG-1. In addition, Saratovsky et al. [49] reported todorokite-like biogenic Mn oxides from *Acremonium* KR21-2 in solid agar media.

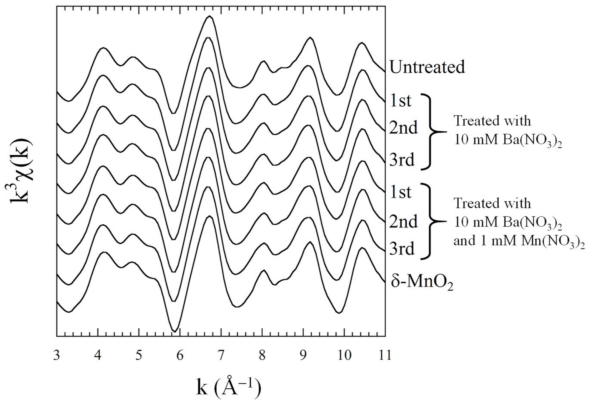

Figure 3. Mn K-edge extended X-ray absorption fine structure spectra for the newly formed biogenic Mn oxides (BMOs) treated with and without 10 mM $Ba(NO_3)_2$ and 1 mM $Mn(NO_3)_2$. δ-MnO_2 was plotted as a reference phyllomanganate for comparison.

The XRD patterns of the newly formed BMOs repeatedly treated in Ba^{2+} and exogenous Mn^{2+} are typical of birnessite (Figure 4). As the initial Ba^{2+} concentration increased, the peak intensities for the (001) and (002) basal reflections also significantly increased, especially the (002) reflection peak. The full width at half maximum (FWHM) of basal reflections for the resulting BMOs narrowed in comparison to those of the newly formed BMOs treated with exogenous Mn^{2+} without Ba^{2+}, indicating tighter layer stacking as the irreversible Ba^{2+} content increased. In addition to Mn K-edge EXAFS results (see above), the XRD results confirmed minor alteration from turbostratic to tightly stacked (well-ordered along the *c*-axis) birnessite, with subsequent irreversible Ba^{2+} accommodation, possibly into the interlayer space. This observation is consistent with the absence of alteration in the diffractogram for exchangeable Ba^{2+} removal using the Cu(II) procedure (Figure S4).

Without exogenous Mn^{2+}, the repeated treatment in Ba^{2+} solutions at 1 and 10 mM significantly weakened the (001) and (002) basal reflection peaks (Figure S5), suggesting that Ba^{2+} sequestration on the "preformed" BMOs increased the disorder in its turbostratic structure along the *c*-axis hosting most reversible Ba^{2+}. Xhaxhiu [50] demonstrated that a chemically synthesized turbostratic Na^{+}–birnessite readily changes to phyllomanganate with disorder along the *c*-axis after treatment in a Ba^{2+} solution. In addition to the loss of the (001) and (002) peaks by the heated (enzymatically inactivated) BMOs upon treatment in Ba^{2+}, even with exogenous Mn^{2+} (Figure 4), we conclude that active Mn oxide formation and coexistence with Ba^{2+} are prerequisites for producing tightly stacked birnessite sheets, with irreversible Ba^{2+} incorporation in the interlayer.

Analysis of the Ba K-edge EXAFS data strongly supports the irreversible Ba^{2+} incorporation into the interlayer of the tight birnessite structure. The newly formed BMOs treated thrice in 10 mM Ba^{2+} with and without exogenous Mn^{2+} (1 mM) displayed similar EXAFS

oscillations (Figure 5), with their radial structural functions (RSFs) indicating Ba–O shells at R + ΔR = 2.1 Å. The newly formed BMOs treated with Ba^{2+} and exogenous Mn^{2+} also exhibited small peaks attributed to the Ba–Mn scattering path at R + ΔR = 3.6 Å. The second shell of Ba–Mn scattering was clearer after the extraction using a 10 mM $Cu(NO_3)_2$ solution for removing exchangeable (reversible) Ba^{2+}. This indicates that the irreversible Ba^{2+} on the BMOs created an inner-sphere complex in association with dehydration. The complex suggests covalent bonding of Ba^{2+} to the oxygen atoms of the MnO_6 octahedra at interlayer sites. This strong Ba^{2+} bonding is probably irreversible, and it stimulated the structure development of tightly stacked birnessite. Further studies are needed to clarify the atomic-level Ba^{2+} incorporation mechanism during enzymatic Mn(II) oxide formation.

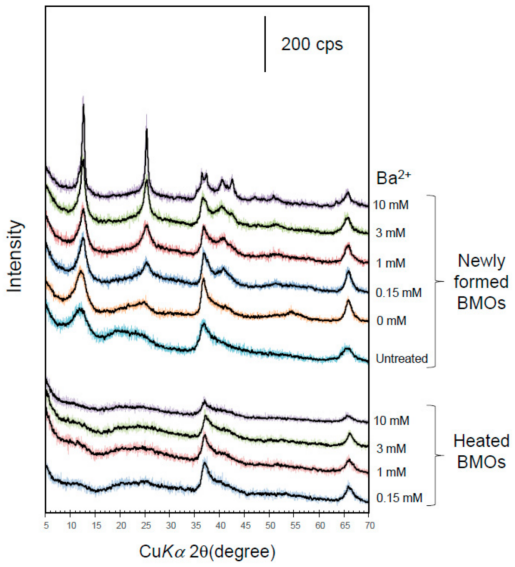

Figure 4. X-ray diffractograms from analysis of the newly formed and heated biogenic manganese oxides (1 mM as Mn) treated thrice with mixtures of $Ba(NO_3)_2$ (0–10 mM) and 1 mM $Mn(NO_3)_2$ in 20 mM HEPES (pH 7.0). The bathing solutions were renewed every 24 h.

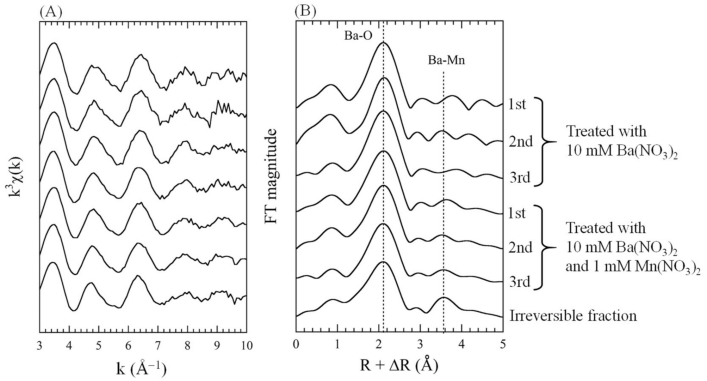

Figure 5. Ba K-edge EXAFS spectra of the newly formed BMOs treated in 10 mM $Ba(NO_3)_2$ with and without 1 mM $Mn(NO_3)_2$, highlighting the (**A**) EXAFS oscillations and (**B**) corresponding radial structural functions (RSFs). The irreversible fraction indicates the Ba^{2+} left on the BMO after extracting the reversible Ba^{2+} fraction using 10 mM $Cu(NO_3)_2$.

3.4. Sr^{2+}, Ca^{2+}, and Mg^{2+} Sequestration by Newly Formed or Heated BMOs Involving Exogenous Mn^{2+}

To determine if irreversible sequestration during active Mn oxide formation is specific for Ba^{2+} or if it is possible for other alkaline earth metal ions, we treated newly formed BMOs (1 mM Mn) thrice in 10 mM Sr^{2+}, Ca^{2+}, or Mg^{2+}, including exogenous 1 mM Mn^{2+} (20 mM HEPES at pH of 7.0). For all alkaline earth metal ions, the exogenous Mn^{2+}

was converted to solid Mn with an efficiency > 97% after every 24 h, with reducible Mn exceeding 89%, confirming retention of the Mn(II) oxidation efficiency (Figure 6). The Sr^{2+} sequestered was 0.31 ± 0.01, 0.40 ± 0.05, and 0.48 ± 0.05 mM after the first, second, and third treatments, respectively, with exchangeable (reversible) Sr^{2+} exceeding 98% (Figure 6 and Table S2). Exchangeable Ca^{2+} also dominated the sequestered Ca^{2+} (>94.5%) with the totals (0.28 ± 0.05, 0.37 ± 0.01, and 0.51 ± 0.03 mM) close to those for Sr^{2+} (Figure 6 and Table S2). However, the sequestered quantities of Mg^{2+} (0.18 ± 0.03, 0.37 ± 0.02, and 0.41 ± 0.01 mM, respectively) were lower, with a higher exchangeable fraction of >82% (Figure 6 and Table S2). These results indicate that the sequestration of these ions on the newly formed BMOs is controlled primarily by reversible sorption, even with simultaneous exogenous Mn^{2+} oxidation. In addition, all BMOs produce XRD patterns typical of turbostratic birnessite, with the (001) and (002) basal peaks broader than those of the tightly stacked birnessite-type BMOs involving irreversible Ba^{2+} (Figure 7). Therefore, the high irreversible sequestration appears to be limited to Ba^{2+}.

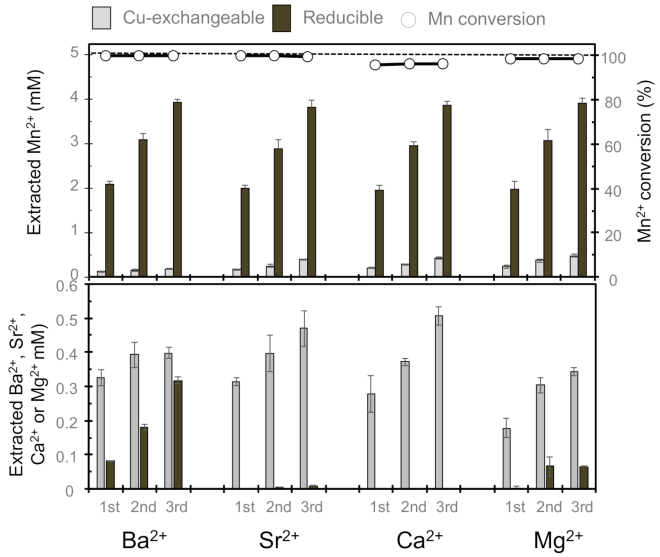

Figure 6. Illustration of the two-step extraction of Ba^{2+} and Mn from the newly formed biogenic manganese oxides during repeated treatment with mixtures of 10 mM $Ba(NO_3)_2$, $Sr(NO_3)_2$, $Ca(NO_3)_2$, or $Mg(NO_3)_2$ with 1 mM $Mn(NO_3)_2$ in 20 mM HEPES (pH of 7.0). The bathing solutions were renewed thrice every 24 h. The conversion (%) from Mn^{2+} to solid Mn is displayed in the top panel.

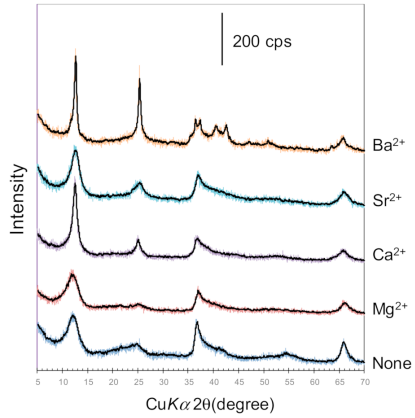

Figure 7. X-ray diffraction analysis of newly formed biogenic manganese oxides (1 mM as Mn) with mixed solutions of 10 mM $Ba(NO_3)_2$, $Sr(NO_3)_2$, $C(NO_3)_2$, or $Mg(NO_3)_2$ with 1 mM $Mn(NO_3)_2$ in 20 mM HEPES (pH 7.0). Bathing solutions were renewed thrice every 24 h.

3.5. Active Mn^{2+} Oxidation Sequestration Selectivity Enhancement for Ba^{2+}

To assess the sequestration selectivity among the alkaline earth metal ions, we conducted competitive sequestration experiments in a solution containing 1 mM Ba^{2+}, 1 mM Sr^{2+}, and 1 mM exogenous Mn^{2+} (20 mM HEPES at pH 7.0) using the newly formed BMOs (1 mM Mn). After three treatments, with renewal of the bathing solution every 24 h, the exogenous Mn^{2+} was converted to the solid phase (>99% efficiency), with reducible Mn dominating (>92.0 ± 0.5%; Figure 8), indicating active Mn oxide formation. The sequestration efficiency for Ba^{2+} was 24.6 ± 1.2%, 12.5 ± 0.3%, and 10.4 ± 0.9% for the first, second, and third treatment (cumulative efficiency 15.8 ± 0.8%), respectively (Table S3). The sequestration efficiencies of 5.5 ± 0.4%, <1%, and <1% (cumulative ~0.7%), respectively, for Sr^{2+} were significantly lower. The two-step extraction produced $Ba^{2+}{}_{seq}/Sr^{2+}{}_{seq}$ molar ratios for the resultant BMO phase ranging from 4.9 to 9.1 (Figure 8D), highlighting a clear increase with renewal of the bathing solution. Similar trends were observed for Ba^{2+}/Ca^{2+} and Ba^{2+}/Mg^{2+} with exogenous Mn^{2+}, with $Ba^{2+}{}_{seq}/Ca^{2+}{}_{seq}$ and $Ba^{2+}{}_{seq}/Mg^{2+}{}_{seq}$ molar ratios increasing from 7.1 to 10.6 and from 13.1 to 31.2, respectively (Figure 8D). Evidently, even in the competitive sequestration experiments, the proportion of irreversible (reducible) Ba^{2+} significantly increased as the exogenous Mn^{2+} progressed (Figure 8B), while the coexisting Sr^{2+}, Ca^{2+}, and Mg^{2+} were sequestered mostly as exchangeable fractions (Figure 8C). For example, the reducible Ba^{2+} increased from 26.6 ± 1.5% to 40.3 ± 0.3% and then to 46.8 ± 0.3%, while exchangeable Sr^{2+} dominated the sequestered Sr^{2+} (>99%) throughout the experiment (Table S3).

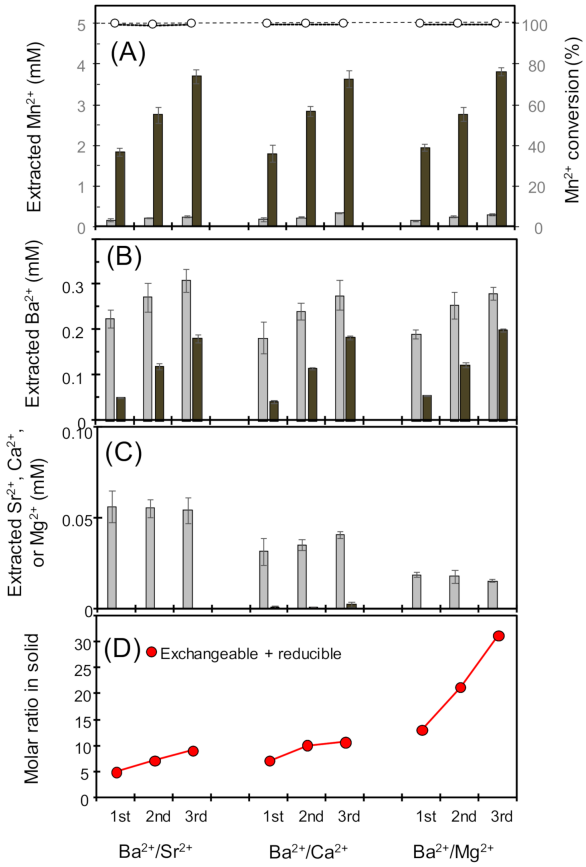

Figure 8. Diagram showing the two-step extraction of (**A**) Mn; (**B**) Ba; and (**C**) Sr, Ca, or Mg from the newly formed biogenic manganese oxides during repeated treatments with mixed solutions of 1 mM $Ba(NO_3)_2$ and 1 mM $Mn(NO_3)_2$ in 20 mM HEPES (pH of 7.0) with 1 mM $Sr(NO_3)_2$, $Ca(NO_3)_2$, or $Mg(NO_3)_2$. The bathing solutions were renewed thrice every 24 h. (**D**) Plot of the Ba/Sr, Ba/Ca, and Ba/Sr molar ratios in the solid phases demonstrating sequestration selectivity.

Competitive sequestration experiments without exogenous Mn^{2+} also revealed that exchangeable Ba^{2+} was dominant in the sequestered Ba^{2+} (>94.4%) (Figure 9B and Table S3), consistent with the Ba^{2+} restricted sequestration experiments. Most Sr^{2+}, Ca^{2+}, and Mg^{2+} sequestered were also in the exchangeable fractions (Figure 9C). The $Ba^{2+}_{seq}/Sr^{2+}_{seq}$, $Ba^{2+}_{seq}/Ca^{2+}_{seq}$, and $Ba^{2+}_{seq}/Mg^{2+}_{seq}$ molar ratios were, however, lower than those with exogenous Mn^{2+}, ranging from 4.3 to 5.1, 4.1 to 5.1, and 5.7 to 6.5, respectively (Figure 9D). Consequently, the reversible Ba^{2+} sequestration by the preformed BMOs caused lower Ba^{2+} selectivity compared to the irreversible Ba^{2+} sequestration into tightly stacked birnessite-type BMOs.

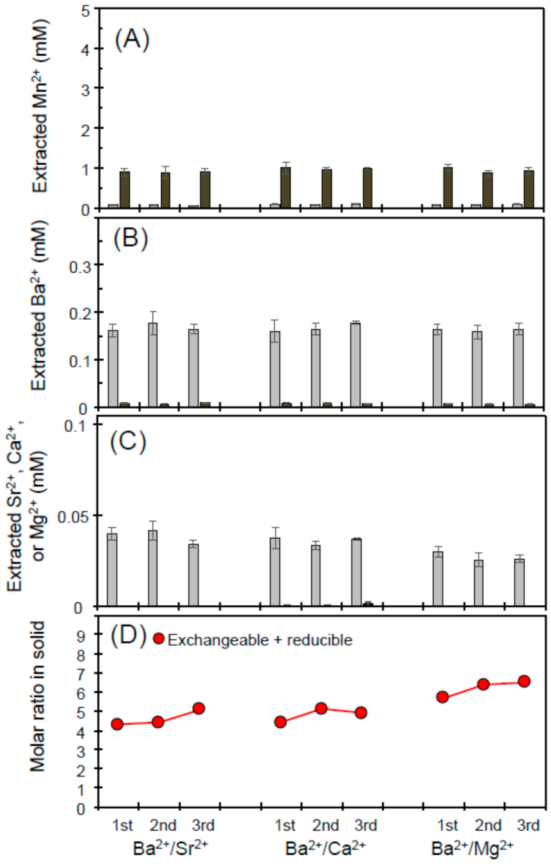

Figure 9. Diagram showing the two-step extraction of (**A**) Mn; (**B**) Ba; and (**C**) Sr, Ca, or Mg from the newly formed biogenic manganese oxides during repeated treatment with mixtures of 1 mM $Ba(NO_3)_2$ and 1 mM $Sr(NO_3)_2$, $Ca(NO_3)_2$, or $Mg(NO_3)_2$ in 20 mM HEPES (pH of 7.0) without exogenous Mn^{2+}. The bathing solutions were renewed thrice every 24 h. (**D**) Plot of the Ba/Sr, Ba/Ca, and Ba/Sr molar ratios in the exchangeable and solid (exchangeable + reducible) phases showing sequestration selectivity.

The XRD patterns of the newly formed BMOs treated thrice in a mixture of 1 mM Ba^{2+} and 1 mM Sr^{2+} resembled those for BMOs treated in the 1 mM Ba^{2+} solution more than those for BMOs treated in the 1 mM Sr^{2+} solution (Figure S6). This confirms that only Ba^{2+} was irreversibly incorporated, even in the competitive sequestration experiments. The biological Ba^{2+} sequestration process is likely in environments with simultaneous supply of Mn^{2+} and Ba^{2+}, which subsequently contributes to Ba^{2+} accumulation in birnessite-type Mn oxides.

4. Conclusions

In this study, we present results showing that irreversible Ba^{2+} sequestration predominates during simultaneous enzymatic Mn oxidation. This process is a likely pathway for

Ba^{2+} sequestration into naturally occurring Mn oxide phases, with microbial (enzymatic) activity occasionally catalyzing the process in the environment. Irreversible sequestration was limited to Ba^{2+}, with Sr^{2+}, Ca^{2+}, and Mg^{2+} characterized by reversible sequestration, thereby explaining the preferential accumulation of Ba^{2+} in Mn oxide phases in the environment. These findings improve understanding of the role of biogenic Mn oxidation in natural Ba^{2+} cycling, particularly under conditions in which microbial Mn(II) oxidation dominates abiotic processes. The insights from this study also highlight the potential of enzymatically active BMOs for scavenging Ba^{2+} from contaminated wastewaters.

Supplementary Materials: The following are available online at https://www.mdpi.com/2075-163X/11/1/53/s1: Figure S1: Mn^{2+} oxidation by newly formed BMOs in $Mn(NO_3)_2$. Figure S2: XRD patterns of newly formed BMOs treated with $Mn(NO_3)_2$. Figure S3: Repeated treatment of newly formed BMOs $Ba(NO_3)_2$. Figure S4: Effect of Cu^{2+}-extraction on XRD patterns of newly formed and heated BMOs. Figure S5: XRD patterns of newly formed BMOs treated with $Ba(NO_3)_2$. Figure S6: XRD patterns of newly formed BMOs treated with mixed solutions of $Ba(NO_3)_2$ and $Sr(NO_3)_2$. Table S1: Data summary of sequestration experiments for Ba^{2+}. Table S2: Data summary of sequestration experiments for Sr^{2+}, Ca^{2+}, or Mg^{2+}. Table S3: Data summary of competitive sequestration experiments.

Author Contributions: Conceptualization, Y.T. and N.M.; methodology, Y.T., K.T. and N.M.; validation, Y.T., S.K., J.C., K.T. and N.M.; formal analysis, S.K. and J.C.; investigation, Y.T., K.T. and N.M.; data curation, Y.T., S.K. and J.C.; writing—original draft preparation, Y.T.; writing—review and editing, Y.T., K.T. and N.M.; visualization, Y.T.; supervision, Y.T.; project administration, Y.T.; funding acquisition, Y.T. All authors have read and agreed to the published version of the manuscript.

Funding: This research was funded by the Japan Society of the Promotion of Science, JSPS KAKENHI, no. 20K12222 (Y.T.).

Institutional Review Board Statement: Not applicable.

Informed Consent Statement: Not applicable.

Data Availability Statement: The data presented in this study are available in the Supplementary Materials (Tables S1–S3).

Acknowledgments: We would like to thank Editage for the editing assistance. The EXAFS measurements were performed with the approval of the Photon Factory, KEK (proposal no. 2018G111) and SPring-8 (proposal no. 2018B1012).

Conflicts of Interest: The authors declare no conflict of interest.

References

1. Suwa, R.; Jayachandran, K.; Nguyen, N.T.; Boulenouar, A.; Fujita, K.; Saneoka, H. Barium toxicity effects in soybean plants. *Arch. Environ. Contam. Toxicol.* **2008**, *55*, 397–403. [CrossRef] [PubMed]
2. Golding, L.A.; McKnight, K.; Binet, M.; Adams, M.; Apte, S.C. Toxicity of dissolved and precipitated forms of barium to a freshwater alga (*Chlorella* sp. 12) and water flea (*Ceriodaphnia dubia*). *Environ. Toxicol. Chem.* **2018**, *37*, 1632–1642. [CrossRef]
3. Lu, Q.; Xu, X.; Xu, Z.; Liang, L.; Shang, L.; Xiao, D.; Zhang, S.; Jiang, Y.; Qiu, G. Barium concentrations and speciation in surface waters collected from an active barium mining area in Guizhou Province, southwestern China. *Environ. Sci. Pollut. Res. Int.* **2018**, *25*, 7608–7617. [CrossRef] [PubMed]
4. Rebello, C.A.; Couperthwaite, S.J.; Millar, G.J.; Dawes, L.A. Coal seam water quality and the impact upon management strategies. *J. Petrol. Sci. Eng.* **2017**, *150*, 323–333. [CrossRef]
5. Warner, N.R.; Christie, C.A.; Jackson, R.B.; Vengosh, A. Impacts of shale gas wastewater disposal on water quality in western Pennsylvania. *Environ. Sci. Technol.* **2013**, *47*, 11849–11857. [CrossRef] [PubMed]
6. Sun, Y.; Wang, D.; Tsang, D.C.W.; Wang, L.; Ok, Y.S.; Feng, Y. A critical review of risks, characteristics, and treatment strategies for potentially toxic elements in wastewater from shale gas extraction. *Environ. Int.* **2019**, *125*, 452–469. [CrossRef] [PubMed]
7. Post, J.E. Manganese oxide minerals: Crystal structures and economic and environmental significance. *Proc. Natl. Acad. Sci. USA* **1999**, *96*, 3447–3454. [CrossRef] [PubMed]
8. Manceau, A.; Kersten, M.; Marcus, M.A.; Geoffroy, N.; Granina, L. Ba and Ni speciation in a nodule of binary Mn oxide phase composition from Lake Baikal. *Geochim. Cosmochim. Acta* **2007**, *71*, 1967–1981. [CrossRef]
9. Bohu, T.; Akob, D.M.; Abratis, M.; Lazar, C.S.; Küsel, K. Biological low-pH Mn(II) oxidation in a manganese deposit influenced by metal-rich groundwater. *Appl. Environ. Microbiol.* **2016**, *82*, 3009–3021. [CrossRef]

10. Tani, Y.; Miyata, N.; Iwahori, K.; Soma, M.; Tokuda, S.; Seyama, H.; Theng, B.K.G. Biogeochemistry of manganese oxide coatings on pebble surfaces in the Kikukawa River System, Shizuoka, Japan. *Appl. Geochem.* **2003**, *18*, 1541–1554. [CrossRef]
11. Manceau, A.; Lanson, M.; Geoffroy, N. Natural speciation of Ni, Zn, Ba, and as in ferromanganese coatings on quartz using X-ray fluorescence, absorption, and diffraction. *Geochim. Cosmochim. Acta* **2007**, *71*, 95–128. [CrossRef]
12. Adams, J.P.; Kirst, R.; Kearns, L.E.; Krekeler, M.P.S. Mn-oxides and sequestration of heavy metals in a suburban catchment basin of the Chesapeake Bay watershed. *Environ. Geol.* **2009**, *58*, 1269–1280. [CrossRef]
13. Sasaki, K.; Kaseyama, T.; Hirajima, T. Selective sorption of Co(II) over Ni(II) using biogenic manganese oxides. *Mater. Trans.* **2009**, *50*, 2643–2648. [CrossRef]
14. Mayanna, S.; Peacock, C.L.; Schäffner, F.; Grawunder, A.; Merten, D.; Kothe, E.; Büchel, G. Biogenic precipitation of manganese oxides and enrichment of heavy metals at acidic soil pH. *Chem. Geol.* **2015**, *402*, 6–17. [CrossRef]
15. Yuan, L.; Sun, L.; Fortin, D.; Wang, Y.; Yin, X. Microscale characterization and trace element distribution in bacteriogenic ferromanganese coatings on sand grains from an intertidal zone of the East China Sea. *PLoS ONE* **2015**, *10*, e0119080. [CrossRef] [PubMed]
16. Tebo, B.M.; Bargar, J.R.; Clement, B.G.; Dick, G.J.; Murray, K.J.; Parker, D.; Verity, R.; Webb, S.M. Biogenic manganese oxides: Properties and mechanisms of formation. *Annu. Rev. Earth Planet. Sci.* **2004**, *32*, 287–328. [CrossRef]
17. Villalobos, M.; Bargar, J.; Sposito, G. Trace metal retention on biogenic manganese oxide nanoparticles. *Elements* **2005**, *1*, 223–226. [CrossRef]
18. Furuta, S.; Ikegaya, H.; Hashimoto, H.; Ichise, S.; Kohno, T.; Miyata, N.; Takada, J. Formation of filamentous Mn oxide particles by the alphaproteobacterium *Bosea* sp. strain BIWAKO-01. *Geomicrobiol. J.* **2015**, *32*, 666–676. [CrossRef]
19. Nelson, Y.M.; Lion, L.W.; Ghiorse, W.C.; Shuler, M.L. Production of biogenic Mn oxides by *Leptothrix discophora* SS-1 in a chemically defined growth medium and evaluation of their Pb adsorption characteristics. *Appl. Environ. Microbiol.* **1999**, *65*, 175–180. [CrossRef]
20. Nelson, Y.M.; Lion, L.W.; Shuler, M.L.; Ghiorse, W.C. Effect of oxide formation mechanisms on lead adsorption by biogenic manganese (hydr)oxides, iron (hydr)oxides, and their mixtures. *Environ. Sci. Technol.* **2002**, *36*, 421–425. [CrossRef]
21. Villalobos, M.; Bargar, J.; Sposito, G. Mechanisms of Pb(II) sorption on a biogenic manganese oxide. *Environ. Sci. Technol.* **2005**, *39*, 569–576. [CrossRef]
22. Toner, B.; Manceau, A.; Webb, S.M.; Sposito, G. Zinc sorption to biogenic hexagonal- birnessite particles within a hydrated bacterial biofilm. *Geochim. Cosmochim. Acta* **2006**, *70*, 27–43. [CrossRef]
23. Miyata, N.; Tani, Y.; Sakata, M.; Iwahori, K. Microbial manganese oxide formation and interaction with toxic metal ions. *J. Biosci. Bioeng.* **2007**, *104*, 1–8. [CrossRef]
24. Meng, Y.T.; Zheng, Y.M.; Zhang, L.M.; He, J.Z. Biogenic Mn oxides for effective adsorption of Cd from aquatic environment. *Environ. Pollut.* **2009**, *157*, 2577–2583. [CrossRef]
25. Sasaki, K.; Uejima, Y.; Sakamoto, A.; Yu, Q.; Ishibashi, J.; Okibe, N.; Hirajima, T. Geochemical and microbiological analysis of Sambe Hot Springs, Shimane Prefecture, Japan. *Res. Geol.* **2013**, *63*, 155–165. [CrossRef]
26. Wang, W.M.; Shao, Z.Z.; Liu, Y.J.; Wang, G.J. Removal of multi-heavy metals using biogenic manganese oxides generated by a deep-sea sedimentary bacterium *Brachybacterium* sp. strain Mn32. *Microbiology* **2009**, *155*, 1989–1996. [CrossRef] [PubMed]
27. Yu, Q.; Sasaki, K.; Tanaka, K.; Ohnuki, T.; Hirajima, T. Zinc sorption during bio-oxidation and precipitation of manganese modifies the layer stacking of biogenic birnessite. *Geomicrobiol. J.* **2013**, *30*, 829–839. [CrossRef]
28. Grangeon, S.; Bataillard, P.; Coussy, S. The nature of manganese oxides in soils and their role as scavengers of trace elements: Implication for soil remediation. In *Environmental Soil Remediation and Rehabilitation*; Van Hullebusch, E.D., Huguenot, D., Pechaud, Y., Simonnot, M.-O., Colombano, S., Eds.; Springer Nature: Cham, Switzerland, 2020; Chapter 7; pp. 399–429. [CrossRef]
29. Chang, J.; Tani, Y.; Naitou, H.; Miyata, N.; Seyama, H. Fungal Mn oxides supporting Mn(II) oxidase activity as effective Mn(II) sequestering materials. *Environ. Technol.* **2013**, *34*, 2781–2787. [CrossRef] [PubMed]
30. Watanabe, J.; Tani, Y.; Chang, J.; Miyata, N.; Naitou, H.; Seyama, H. As(III) oxidation kinetics of biogenic manganese oxides formed by *Acremonium strictum* strain KR21-2. *Chem. Geol.* **2013**, *347*, 227–232. [CrossRef]
31. Tojo, F.; Kitayama, A.; Miyata, N.; Okano, K.; Fukushima, J.; Suzuki, R.; Tani, Y. Molecular cloning and heterologous expression of manganese(II)-oxidizing enzyme from *Acremonium strictum* strain KR21-2. *Catalysts* **2020**, *10*, 686. [CrossRef]
32. Chang, J.; Tani, Y.; Naitou, H.; Miyata, N.; Tojo, F.; Seyama, H. Zn(II) sequestration by fungal biogenic manganese oxide through enzymatic and abiotic processes. *Chem. Geol.* **2014**, *383*, 155–163. [CrossRef]
33. Chang, J.; Tani, Y.; Naitou, H.; Miyata, N.; Seyama, H.; Tanaka, K. Cobalt(II) sequestration on fungal biogenic manganese oxide enhanced by manganese(II) oxidase activity. *Appl. Geochem.* **2013**, *37*, 170–178. [CrossRef]
34. Chang, J.; Tani, Y.; Naitou, H.; Miyata, N.; Seyama, H.; Tanaka, K. Sequestration of Cd(II) and Ni(II) ions on fungal manganese oxides associated with Mn(II) oxidase activity. *Appl. Geochem.* **2014**, *47*, 198–208. [CrossRef]
35. Inthorn, D.; Tani, Y.; Chang, J.; Naitou, H.; Miyata, N. Magnetically modified fungal Mn oxides with high sequestration efficiency for simultaneously removing multiple heavy metal ions from wastewater. *J. Environ. Chem. Eng.* **2014**, *2*, 1635–1641. [CrossRef]
36. Zheng, H.; Tani, Y.; Naitou, H.; Miyata, N.; Tojo, F.; Seyama, H. Sequestration of La^{3+} by fungal manganese oxides and the effect of Mn(II) oxidase activity. *J. Environ. Chem. Eng.* **2017**, *5*, 735–743. [CrossRef]
37. Zheng, H.; Tani, Y.; Naitou, H.; Miyata, N.; Tojo, F. Oxidative Ce^{3+} sequestration by fungal manganese oxides with an associated Mn(II) oxidase activity. *Appl. Geochem.* **2016**, *71*, 110–122. [CrossRef]

38. Suzuki, R.; Tani, Y.; Naitou, H.; Miyata, N.; Tanaka, K. Sequestration and oxidation of Cr(III) by fungal Mn oxides with Mn(II) oxidizing activity. *Catalysts* **2020**, *10*, 44. [CrossRef]
39. Miyata, N.; Tani, Y.; Iwahori, K.; Soma, M. Enzymatic formation of manganese oxides by an *Acremonium*-like hyphomycete fungus, strain KR21-2. *FEMS Microbiol. Ecol.* **2004**, *47*, 101–109. [CrossRef]
40. Miyata, N.; Tani, Y.; Maruo, K.; Tsuno, H.; Sakata, M.; Iwahori, K. Manganese(IV) oxide production by *Acremonium* sp. strain KR21-2 and extracellular Mn(II) oxidase activity. *Appl. Environ. Microbiol.* **2006**, *72*, 6467–6473. [CrossRef]
41. Tani, Y.; Miyata, N.; Ohashi, M.; Ohnuki, T.; Seyama, H.; Iwahori, K.; Soma, M. Interaction of inorganic arsenic with biogenic manganese oxide produced by a Mn-oxidizing fungus, strain KR21-2. *Environ. Sci. Technol.* **2004**, *38*, 6618–6624. [CrossRef]
42. Stumm, W.; Morgan, J.J. *Aquatic Chemistry. Chemical Equilibria and Rates in Natural Waters*, 3rd ed.; John Wiley & Sons, Inc.: New York, NY, USA, 1995; pp. 976–983.
43. Rosson, R.A.; Nealson, K.H. Manganese binding and oxidation by spores of a marine bacillus. *J. Bacteriol.* **1982**, *151*, 1027–1034. [CrossRef] [PubMed]
44. De Vrind, J.P.; De Vrind-de Jong, E.W.; De Voogt, J.W.; Westbroek, P.; Boogerd, F.C.; Rosson, R.A. Manganese oxidation by spores and spore coats of a marine *Bacillus* species. *Appl. Environ. Microbiol.* **1986**, *52*, 1096–1100. [CrossRef] [PubMed]
45. Watanabe, J.; Tani, Y.; Miyata, N.; Seyama, H.; Mitsunobu, S.; Naitou, H. Concurrent sorption of As(V) and Mn(II) during biogenic manganese oxide formation. *Chem. Geol.* **2012**, *306–307*, 123–128. [CrossRef]
46. Reimann, C.; De Caritat, P. *Chemical Elements in the Environment: Factsheets for the Geochemist and Environmental Scientist*; Springer: Berlin/Heidenburg, Germany, 1998; p. 397.
47. Grangeon, S.; Lanson, B.; Miyata, N.; Tani, Y.; Manceau, A. Structure of nanocrystalline phyllomanganates produced by freshwater fungi. *Am. Mineral.* **2010**, *95*, 1608–1616. [CrossRef]
48. Webb, S.M.; Fuller, C.C.; Tebo, B.M.; Bargar, J.R. Determination of uranyl incorporation into biogenic manganese oxides using X-ray absorption spectroscopy and scattering. *Environ. Sci. Technol.* **2006**, *40*, 771–777. [CrossRef]
49. Saratovsky, I.; Gurr, S.J.; Hayward, M.A. The structure of manganese oxide formed by the fungus *Acremonium* sp. strain KR21-2. *Geochim. Cosmochim. Acta* **2009**, *73*, 3291–3300. [CrossRef]
50. Xhaxhiu, K. Synthetic birnessites and buserites as heavy metal cation traps and environmental remedies. *J. Metal. Nanotechnol.* **2015**, *3*, 23–32.